A SHORT CAVITY SEMICONDUCTOR LASER SYSTEM: DYNAMICS BEYOND LANG-KOBAYASHI

Michael Peil
Institute of Applied Physics
Darmstadt University of Technology
Germany
michael.peil@physik.tu-darmstadt.de

Ingo Fischer
Institute of Applied Physics
Darmstadt University of Technology
Germany
ingo.fischer@physik.tu-darmstadt.de
now: Dept. of Appl. Physics and Photonics
Vrije Universiteit Brussel, Belgium

Wolfgang Elsäßer
Institute of Applied Physics
Darmstadt University of Technology
Germany
elsaesser@physik.tu-darmstadt.de

Abstract

We present experiments on the dynamics of a multimode semiconductor laser (SL) system subject to moderate optical feedback operating in the short cavity regime (SCR). For the ratio between the external cavity length and the optical laser cavity length, we have chosen simple ratios between 2 and 4, fulfilling resonant coupling conditions for the solitary laser modes. We study the influence of injection current and feedback phase on the dynamics under such conditions. As in the case of the SCR, we find a cyclic scenario of the dynamics depending on the feedback phase. Within one cycle, the dynamics evolves from stable emission via periodic states to chaos. In contrast to Lang-Kobayashi SCR-dynamics, the chaotic dynamics in this system involves a remarkably large number of longitudinal modes - easily exceeding 100 - leading to an optical bandwidth of $\sim$7 nm. This dynamics is associated with broadband intensity rf-spectra with ~ 6 GHz bandwidth. We discuss this behavior in the context of spectral dynamics and modal overlap leading to strong interactions among the modes, demonstrating how this behavior goes beyond the Lang-Kobayashi (LK-) description. Our results suggest that refined models are desired to gain deeper insight into the nonlinear dynamics of resonantly coupled multimode SL-systems.

Key words

semiconductor lasers, delay dynamics, coherence collapse, multimode emission, resonant coupling

1 Introduction

Over the last two decades, the dynamics of semiconductor lasers (SLs) subjected to delayed optical feedback has been attracting much attention in the field of nonlinear dynamics. The attractiveness of these systems is substantiated by the rich variety of nonlinear dynamical phenomena that have been found because of their emission dynamics. For a recent overview over various dynamical phenomena, we refer to (Krauskopf B., 2000) and references cited therein. The occurrence of the complex dynamics can be mainly attributed to the following two SL characteristics. Firstly, SL-systems with delayed optical feedback are delay systems, which are, mathematically, infinite dimensional. Therefore, they offer the potential to exhibit high-dimensional dynamics. Secondly, the interaction among the intense laser field inside the SL cavity and the semiconductor medium gives rise to a pronounced inherent nonlinearity in these systems (Henry, 1982; Heil *et al.*, 1999). This nonlinearity is typically described by the so-called α-parameter. The combination of both delayed feedback and an inherent strong nonlinearity provides potential for high-dimensional chaotic intensity dynamics and, finally, evokes the multitude of dynamical phenomena which have been observed. To date, several of the dynamics phenomena occurring in delay systems are still not fully understood. One reason lies in the fact that an analytical treatment of delay systems is very demanding. In this context, well-controllable SL-systems with delayed feedback have been proven as excellent experimental systems for studying delay dynamics. Moreover, nonlinear dynamics of such SL-systems can be harnessed, offering perspectives for novel technologies, e.g. for chaotic light detection and ranging (CLIDAR) (Lin and Liu, 2004) or encrypted communications (Larger and Goedgebuer, 2004; Donati and Mirasso, 2002).

Until recently, research has mainly focused on systems with external cavities $\mathrm{L_{EC}}$ being sufficiently longer than the laser cavity $\mathrm{L_L}$ (Lang and Kobayashi, 1980; Mørk *et al.*, 1988; Mørk *et al.*, 1992; vanTartvijk *et al.*, 1995; Lenstra, 1997; Heil *et al.*, 2001). It has turned out that most of the dynamics of such systems are captured by models based on the Lang-Kobayashi (LK) SL rate equations (Lenstra, 1997; Fischer *et al.*, 1996; Heil *et al.*, 1999). In that sense, the LK-equations have become an established foundation for

modeling SL-systems. However, the LK-equations are based on several assumptions, which are not fulfilled in the main. Two restrictive assumptions are that the model only accounts for one single longitudinal laser mode and, furthermore, that spatial dependencies in the solitary laser cavity are disregarded in this mean-field model. Nevertheless, further modes and spatial dependencies might become relevant for certain systems. For those conditions, multimode extensions to the LK-equations have been proposed accounting for lasing and coupling of several longitudinal modes (Sukow *et al.*, 1999; Yousefi *et al.*, 2003; Koryukin and Mandel, 2004). However, these models also have their limits of validity and cannot be applied in general. Traveling wave models present a promising and powerful alternative for modeling the dynamics of SL-systems, since they can account for spatial effects. However, they imply more demanding mathematical handling (Tromborg *et al.*, 1997; Duarte and Solari, 1997; Möhrle *et al.*, 2001). We will show that SL-systems with properties far beyond the validity of a LK-description can reveal interesting dynamics phenomena which can give further insight into the properties of complex nonlinear systems in general. In addition, the interesting characteristics of these systems offer potential for technical applications.

In this context, we introduce a multimode SL-system which clearly violates the main assumptions, being negligibility of spatial extension of the laser cavity and single mode operation. Firstly, and in contrast to conventional LK SL-systems, in the presented system the lengths of $\mathrm{L_{EC}}$ and $\mathrm{L_L}$ are of comparable size. Secondly, we additionally introduce resonant coupling conditions between the longitudinal modes. As we will demonstrate, the combination of both features can effect pronounced optical broadband dynamics which are induced by numerous strong interacting longitudinal modes. In the following, we present and analyze the dynamics of this interesting system in detail. The outline of the paper is as follows.

In section 2, we introduce the SL-system and describe the experimental setup which we utilize for characterization of its dynamics. Then, we demonstrate how strong coupling between the longitudinal modes can be achieved by resonant cavity conditions. In section 3, we study the influence of the relevant system parameters on the dynamics. These parameters are the pump current and the feedback phase. For variation of both parameters, we find a cyclic scenario with dynamics evolving from stable emission to periodic states, then to chaos, and, again, to stable emission. We give evidence that for high pump parameters, we are able to achieve broadband chaotic intensity dynamics with an optical bandwidth exceeding 7 nm. We point out that easily more than 100 longitudinal modes are involved in the dynamics. Therefore, we analyze this extraordinary broadband dynamics in detail in section 4. We present results for spectrally resolved measurements which provide insight into the spectral components of the dynamics. Afterwards, we discuss the spectral dynamics, motivating new models which reveal the relevant mechanisms determining the characteristic dynamics of the system. Finally, we draw some conclusions in section 5.

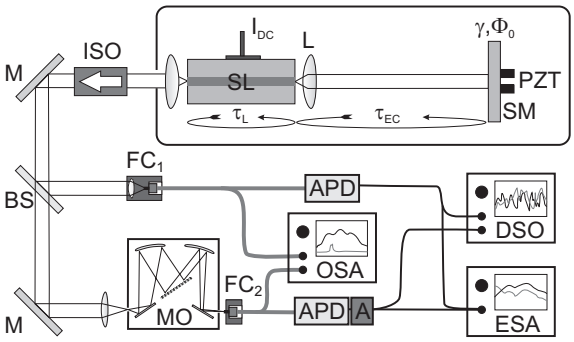

Figure 1. Experimental setup for the multimode semiconductor laser feedback system.

2 Experimental Setup

In this section, we introduce the SL-system allowing for exceptional optical broadband multimode dynamics and illustrate the experimental setup applied for the analysis of the dynamical characteristics of the system. A scheme of the experimental setup is depicted in Figure 1. In this figure, the SL-system is framed by a black line which is located in the upper half of the figure, while the detection branch is mainly sketched in the lower half of the figure. The central device of the system is a ridge waveguide semiconductor laser emitting at a center wavelength of 785 nm. The laser has been selected with respect to a broad and flat gain profile and a small spectral spacing of the longitudinal modes. The length of the laser cavity is $\mathrm{L_L} = 1.6\,\mathrm{mm}$ and the effective refractive index of the gain material of the SL is approximately n = 3.7. Consequently, the longitudinal mode spacing amounts to 25.3 GHz. In order to guarantee well-defined operation conditions, the laser is pumped by an ultra-low-noise DC-current source and its temperature is controlled and stabilized to better than 0.01 K. The light emitted from the right facet of the SL is collimated by a lens (L) and propagates towards a semitransparent mirror (SM) with a reflectivity R. A part of the light is reflected from the SM and is reinjected into the laser after the delay time $\tau_{\mathrm{EC}} = 2\,\mathrm{L_{EC}}/c$, and with the phase (difference) $\Phi_0 = \Phi(t) - \Phi(t-\tau)$. Here, $\mathrm{L_{EC}}$ stands for the length of the external cavity, and c for the speed of light in air, while γ denotes the feedback ratio defined as the ratio between the power of the light coupled back into the laser cavity and the power emitted at the front (right) facet of the laser. In the experiments, the ratio between $\mathrm{L_{EC}}$ and the effective laser length $\mathrm{L_{L,eff}} = \mathrm{n\,L_L}$ has been chosen between 2 and 4. This corresponds to external cavity round-trip frequencies of $6.3\,\mathrm{GHz} \leq \nu_{\mathrm{EC}} \leq 12.7\,\mathrm{GHz}$. The round-trip fre-

quency of the laser cavity amounts to $\nu_{\mathrm{L}} = 25.3\,\mathrm{GHz}$. For such short external cavity length, the Short Cavity Regime (SCR) requirement (Heil *et al.*, 2001; Heil *et al.*, 2003) is always fulfilled, since the external cavity round-trip frequency $1/\tau_{\mathrm{EC}}$ is sufficiently larger than the relaxation oscillation frequency ν_{RO} of the SL, which is always smaller than 3.3 GHz for the accessible pump currents. Under these conditions, the key parameters of the system determining the dynamical behavior are the delay time τ_{EC}, the feedback ratio γ, the pump current $\mathrm{I_{DC}}$ and the feedback phase Φ_0. These parameters can be varied by changing $\mathrm{L_{EC}}$, replacing the SM by one with different reflectivity R, by varying $\mathrm{I_{DC}}$ and by shifting the SM on sub-wavelength scale with a piezo-electric transducer (PZT), respectively. The light emitted from the rear facet of the laser is sent to the detection branch, which is isolated by an optical isolator (ISO) in order to prevent influence from unwanted back-reflections of the detection branch. At the beam splitter (BS), a part of the total intensity is coupled out into a fiber at the fiber coupler ($\mathrm{FC_1}$) and further split into two fractions for analysis. One part is detected by a 12 GHz photo detector (APD), whose output is monitored on a 4 GHz bandwidth digital storage oscilloscope (DSO), and an (electrical) rf-spectrum analyzer (ESA) with 18 GHz bandwidth. The other part of the light is analyzed with an optical grating spectrum analyzer with a resolution of 24 GHz. The light propagating through the BS, is coupled to a grating monochromator (MO) where it is spectrally filtered allowing for analysis of the emission dynamics of selected optical spectral regions. In the following, we will call these measurements spectrally resolved measurement, since the optical spectral bandwidth of the selected region is sufficiently smaller than the full optical spectral bandwidth of the total emission. After passing through the MO, the light is coupled into a fiber at $\mathrm{FC_2}$ for detection. The spectral bandwidth (3 dB) of the filtered light amounts to approximately 170 GHz, which is equivalent to an interval comprising 7 longitudinal modes. The center wavelength of the spectrally filtered light can be tuned over the whole emission spectrum of the SL-system. In analogy to the detection of the full bandwidth intensity signal, the detection apparatus for the spectrally filtered signal is identical, except for an additional rf-amplifier (A) inserted after the APD accounting for the reduced intensity due to spectral filtering, and additional losses due to lower coupling efficiency at $\mathrm{FC_2}$.

Before presenting the experimental characterization of the dynamics of the SL-system, we first motivate a particular choice of external cavity lengths. Namely, we realize resonant coupling of the longitudinal modes of the SL for which we are able to achieve chaotic multimode dynamics with an extraordinary high optical bandwidth. Subsequently, we experimentally characterize the total intensity dynamics of the SL-system in dependence on the pump current and the feedback phase Φ_0.

2.1 Resonant Cavities Condition

The coupling conditions between the laser- and the external cavity are of crucial importance in a multimode SL-system with optical feedback, since they influence the interactions between the lasing modes and, consequently, the dynamics of the total system. In such a double cavity system, resonant coupling is a distinguished condition, in particular when the lengths of the resonators are of comparable size. Under these circumstances, which are realized in this short cavity setup, best coupling conditions are accomplished when the round-trip frequencies between both cavities, the laser cavity ($\nu_{\mathrm{L,eff}}$) and the external cavity (ν_{EC}), fulfill the resonance condition $\nu_{\mathrm{L,eff}}/\nu_{\mathrm{EC}} = \mathrm{N}$, with N being an integer number. For this prerequisite, both resonators strongly couple and adjacent longitudinal modes are equally supported in the gain medium (laser cavity) allowing for substantial coupling between longitudinal modes. Depending on the gain profile, numerous longitudinal modes may be excited in the SL-system offering potential for dynamics with high optical bandwidth. However, fractional ratios of $\nu_{\mathrm{L,eff}}/\nu_{\mathrm{EC}}$ fulfill also similar, although weaker, resonance conditions. In particular, conditions satisfying $\nu_{\mathrm{L,eff}}/\nu_{\mathrm{EC}} = (2N+1)/2$, are also good coupling conditions of the family sufficing fractional resonance conditions. For these conditions every next but one longitudinal mode is supported in the gain medium in a similar manner as for the integer resonance condition, while the modes in between are considerably less supported. Therefore, in this case, the mode spacing between every next but other mode is of importance for the dynamics. The corresponding frequency can be considered as mode spacing frequency of a resonator of half the length of the original effective laser cavity, $\nu'_{\mathrm{L',eff}} = 2\,\nu_{\mathrm{L,eff}}$. For this frequency, in turn, an integer resonance condition is accomplished, being $N' = \nu'_{\mathrm{L',eff}}/\nu_{\mathrm{EC}}$. This situation differs from the original integer resonance condition only in the sense that the frequency spacing of supported modes is larger, which reduces the coupling strength between the supported modes.

In the experiments, we tune $N = \mathrm{L_{EC}}/\mathrm{L_{L,eff}}$ in a range between 2 and 4. We note that we find equivalent good coupling conditions for ratios of 2, 3 and 4, as well as for ratios of 2.5 and 3.5. However, in the experiments presented, we choose a ratio of 2.5, since the larger spectral spacing of the supported modes facilitates better control over the dynamics. This property is especially helpful when studying the onset of dynamics and the emergence of dynamics scenarios. We point out that the results obtained for the dynamics for a ratio of 2.5 agree to those obtained for a ratio of 3, except for minor quantitative differences with respect to the dependence on the control parameters. In the next section, we analyze the emergence of dynamics in the SL-system in detail and give evidence that for resonant coupling we are able to achieve chaotic intensity dynamics with an extraordinarily high optical bandwidth of several nanometers.

3 Scenarios of the Dynamics of the System

In the previous section, we have motivated our choice of the external cavity length being $L_{EC} = 2.5\,L_{L,eff}$. With this condition, we have realized two distinct fundamental preconditions for the behavior of the dynamics of the system. Firstly, as we have seen in the previous section, the system fulfills the SCR-requirement due to the ratio of $\nu_{EC}/\nu_{RO} > 1$. Therefore, the short external cavity SL-system is still a delay system and, hence, it is mathematically infinite dimensional offering the potential for high-dimensional dynamics. Secondly, an additional and new fundamental precondition lies in the fact that the round-trip time inside the short external cavity, $\tau_{EC} \approx 100\,\mathrm{ps}$, is of comparable size as the round-trip time in the laser cavity, being $\tau_L = c/2L_{L,eff} \approx 40\,\mathrm{ps}$. This property implies that adjacent longitudinal laser modes resonantly couple, since they are only separated by about 2 - 3 external cavity modes. Therefore, the fixed points structure of the system is a global one and fundamentally different if compared to multimode LK-systems, in which fix points belonging to individual longitudinal modes can be regarded as being almost independent.

In the following, we demonstrate that interesting broadband dynamics can be discovered because of the specific properties of this short external cavity SL-system. We analyze the characteristics of the dynamics and identify the pump current I_{DC} and the feedback phase Φ_0 as major control parameters. Henceforth, we study their influence on the dynamical properties of the SL-system.

3.1 Influence of the Pump Current

In this subsection, we investigate the dependence of the dynamics on the pump current. A more significant measure than the absolute pump current is the pump parameter (P) which we define as the ratio between the pump current I_{DC} and the solitary laser threshold current (I_{th}), $P = I_{DC}/I_{th}$. Here, the solitary threshold current is $I_{th} = 45.72\,\mathrm{mA}$. In the experiment, we have set the feedback ratio to $\gamma = 0.16$, inducing a threshold reduction of 6.9 % with respect to the solitary laser threshold. For these conditions, we increase the pump parameter from P = 0 to P ≈ 3.

Starting at P = 0, we find the onset of dynamics for P = 0.93. For such small values of the pump parameter, the dynamics consists of slow intensity fluctuations comprising frequencies of up to several hundred MHz. However, the intensity fluctuations are not equally distributed, but cluster around a peak frequency. This peak frequency increases as the pump parameter is increased. As an example for such dynamics, in Figure 2 a) we present a rf-spectrum of the dynamics obtained for a pump parameter of P = 0.96. We note that the peak frequency of the slow intensity fluctuation does not increase continuously for incrementing pump parameter. Instead, we find a (cyclic) scenario for increasing pump parameter on a scale of $\Delta P \approx 0.1$. In this scenario, the dynamics evolves from stable emission to slow intensity fluctuations, which start to cluster giving rise to a distinct peak, as depicted in Figure 2 a). Then, clustering breaks up and the emission becomes stable again. However, the average peak frequency of the dynamics increases continuously for incrementing pump current. For this feedback ratio, approximately 2 cycles of this scenario can be found until the dynamics change for pump levels of about P = 1.2. At this level, an additional higher frequency component emerges at 2.7 GHz, which is not directly related to the relaxation oscillation frequency ν_{RO} of the solitary SL, since $\nu_{RO} \approx 0.6\,\mathrm{GHz}$. Further increasing the pump parameter, the low frequency part of the dynamics becomes less and less pronounced, until it vanishes completely, while the new higher frequency component dominates the emergence of the dynamics. However, the property of the dynamics to evolve cyclically, mediating between stable emission and dynamics, not only persists, but becomes more and more pronounced.

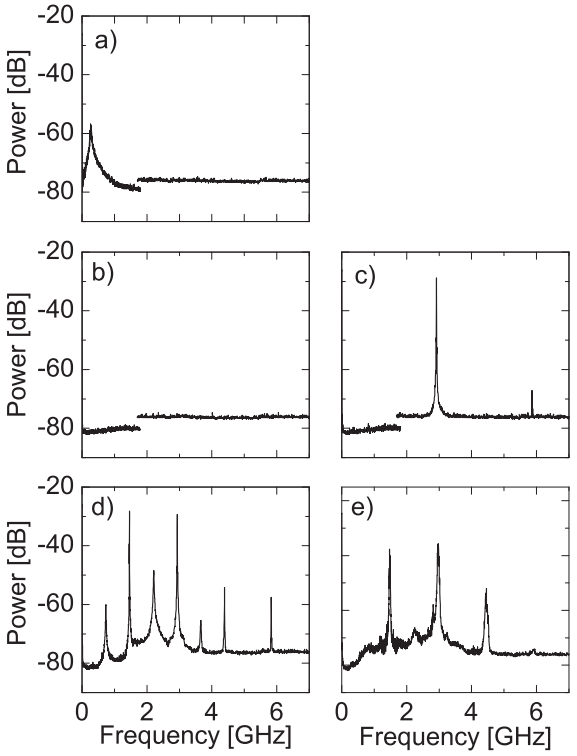

Figure 2. rf-spectra of the intensity dynamics in dependence on the pump parameter P. Figure a) exemplarily shows typical dynamics for low pump levels near laser threshold, here at P = 0.96. For intermediate pump levels and increasing pump parameter, we find a cyclic scenario evolving from stable emission in b), to periodic states in c) and d), to chaotic dynamics e), and, again, to stable emission. The feedback ratio is moderate, $\gamma = 0.16$, and the pump parameters are: a) P = 0.96, b) P = 1.33, c) P = 1.36, d) P = 1.38, and e) P = 1.40.

An example of one characteristic cyclic scenario for intermediate pump parameters is presented in Figure 2. Stable emission is achieved for a pump parameter of P = 1.33. As expected, the corresponding rf-spectrum, which is depicted in Figure 2 b), does not give rise to

any intensity dynamics. We note that the step in the rf-spectra at 1.7 GHz originates from the higher noise level of the electrical spectrum analyzer for the upper detection band for higher frequencies. Increasing the pump level slightly, the intensity starts to oscillate periodically at a frequency of 2.91 GHz. This oscillation becomes more pronounced and slightly shifts to higher frequencies, as the pump parameter is incremented to P = 1.36. In the rf-spectra in Figure 2 c), we identify a peak corresponding to the fundamental frequency at 2.92 GHz and a weakly pronounced peak of the second harmonic at 5.84 GHz. In comparison, the relaxation oscillation frequency of the solitary laser is $\nu_{\mathrm{RO}} \approx 1.5\,\mathrm{GHz}$. With further incrementing the pump parameter, we find a period doubling bifurcation scenario, which becomes clear from the rf-spectrum illustrated in Figure 2 d). The corresponding pump parameter is P = 1.38. For this pump level, we have already reached a period 4 state of the dynamics. Due to this period doubling cascade, we expect chaotic dynamics for higher pump parameters. Indeed, chaotic dynamics can be achieved for P = 1.4, which we demonstrate with the rf-spectrum depicted in Figure 2 e). It becomes clear from the figure that the peaks related to the originally periodic dynamics are significantly broadened. Now, the rf-spectrum reveals an extended bandwidth of the dynamics of ~ 5 GHz reflecting chaotic dynamics. We note that at the onset of chaos the optical spectrum does not give evidence for multimode dynamics. In this sense, at the onset of chaos, the dynamics becomes locally chaotic. As we will demonstrate later on, this property drastically changes for fully developed chaos at higher pump parameters, where the optical spectrum features distinct multimode dynamics. An additional interesting property of the period doubling route to chaos can be identified from the rf-spectrum as presented in Figure 2 e). With increasing pump parameter and, hence, progressing into the chaotic regime, we find the inverse cascade. In particular, the residuals of the period 4 peaks are strongly suppressed in Figure 2 e). Finally, we find that with further increasing pump parameter, the cycle is completed and the chaotic dynamics suddenly disappear and the steady emission state is reached again. We note that we observe hysteresis for this transition between the chaotic and the steady state for increasing and decreasing pump parameter.

The results obtained for intermediate pump parameters indicate that with increasing pump parameter the chaotic dynamics comprise a growing number of longitudinal modes extending the optical bandwidth of the dynamics. Therefore, we have increased the pump parameter substantially, in order to verify if the SL-system offers potential for generation of pronounced chaotic multimode dynamics with high optical bandwidth. Additionally, and in order to support the coupling between adjacent longitudinal modes, we have slightly increased the feedback rate to $\gamma = 0.18$. For this feedback ratio we measure a threshold reduction of 7.5 %. We have adjusted the pump parameter to

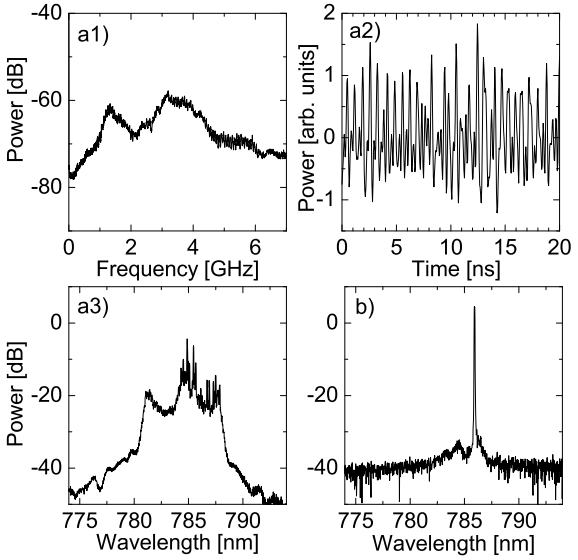

Figure 3. Optical broadband dynamics achieved for high pump parameter P = 3.28 and moderate feedback ratio $\gamma = 0.18$. The rf-spectrum of the intensity dynamics, which are depicted in a1), reveals broadband chaotic dynamics. A 20 ns long segment of the corresponding time series is presented in Figure a2), while Figure a3) demonstrates pronounced multimode dynamics manifesting in the broadband optical spectrum. The optical spectrum for single mode emission, which is obtained for a minor change of the pump parameter of $\Delta \mathrm{P} = -0.03$, is presented in Figure b).

P = 3.28, for which we find pronounced chaotic dynamics. The results are summarized in Figure 3. Figure 3 a1) depicts the rf-spectrum of the dynamics. The continuous spectrum reveals pronounced chaotic intensity dynamics with a bandwidth slightly exceeding 6 GHz. Furthermore, the spectrum does not reveal remains of periodic frequencies stemming from the period doubling scenario as we have seen for lower pump levels in Figure 2 e). In contrast to the pronounced period doubling scenario for small pump parameters, the transition for high pump parameters from the steady state to chaotic dynamics takes place in a very small interval. However, two different regions can be identified in the rf-spectrum. First, there is a broad peak at around 1.3 GHz, which cannot be directly assigned to a characteristic frequency of the system. The second characteristic is a very broad hump with a maximum near 3.2 GHz, which might be related to ν_{RO}, being 3.06 GHz for this pump parameter. A 20 ns long segment of the time series is presented in Figure 3 a2), illustrating the irregular intensity fluctuations of the SL-system on sub-ns time scale. The corresponding optical spectrum is presented in Figure 3 a3). In contrast to the behavior for small pump parameters, the optical spectrum for chaotic dynamics for high pump parameters reveals an extraordinarily high spectral bandwidth of more than 7 nm. Since the spacing of the longitudinal modes amounts to 52 pm, the number of modes involved in the dynamics exceeds 130. A distinct fea-

ture of the broadband optical spectrum is its trident like envelope. Additional experiments have verified that misalignment of the external cavity or dispersion effects in the SL material can be excluded as mechanisms. Therefore, this property seems to be a general property for the optical broadband multimode dynamics of this system. Furthermore, we note that only for resonant coupling conditions, we are able to achieve such conspicuous optical broadband chaotic dynamics. In order to highlight the dramatic increase in the optical bandwidth, in Figure 3 b), we illustrate an optical spectrum for stable emission for comparison. In order to achieve this state, we have decremented the pump level by $\Delta \mathrm{P} = 0.03$. However, we can also increase the pump level in order to reach this state, since the characteristic property of the dynamics evolving cyclically for increasing (and decreasing) pump level persists also for high pump levels.

A possible explanation for the scenario being cyclic can be found in the indirect influence of the pump parameter on the feedback condition. When increasing the pump parameter, we slightly increase $\mathrm{L_{L,eff}}$ because of thermal effects. For an increase of $\mathrm{L_{L,eff}}$, on the other hand, the gain maximum shifts to longer wavelengths causing a red-shift of the emission wavelength. The result is a small decrease of the feedback phase. Since the system operates in the SCR, the feedback phase Φ_0 is a crucial parameter for the dynamics (Heil *et al.*, 2001; Heil *et al.*, 2003). Whether this consideration explains the origin of the cyclic nature of the scenario and whether a feedback phase can be properly defined in a such a pronounced multimode system, will be discussed in the next subsection.

3.2 Influence of the Feedback Phase

The considerations given at the end of the previous subsection indicate that the phase of the feedback might be the relevant parameter for the occurrence of the cyclic scenario. In order to clarify this question, we study the effect of small changes of the length of the external cavity on the dynamics. In the experiments, we vary the length of the external cavity on subwavelength scale utilizing a piezo transducer (PZT). This results in a change of the phase of the feedback. We note that for resonant coupling conditions, a proper feedback phase Φ_0 is defined. Due to the resonance condition, the feedback phases are the same for all supported longitudinal modes. We have verified that the deviations from this consideration induced by dispersion in the laser medium are negligible.

Figure 4 depicts the rf-spectra of typical dynamics for different values of the feedback phase Φ_0. Here, we have chosen a moderate pump parameter of P = 3.06 and a moderate feedback rate, being $\gamma = 0.16$. At the beginning of the experiment, we adjust for steady emission, which is presented by the flat rf-spectrum depicted in Figure 4 a). For this condition, we associate the feedback phase with $\Phi_0 = 0$. In advance, we highlight that we have found a cyclic scenario depending on

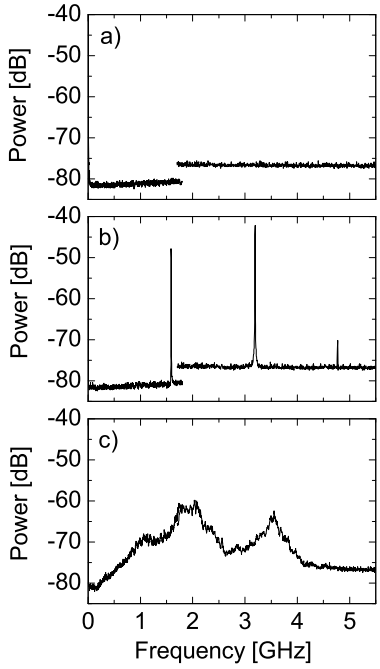

Figure 4. rf-spectra of characteristic dynamics of the π-cyclic scenario for decreasing feedback phase Φ_0. The phase condition for continuous emission, illustrated in Figure a), has been assigned to the phase value $\Phi_0 = 0\,\pi$. Period two dynamics for $\Phi_0 = -0.24\,\pi$, evolving through a period doubling route to chaos, is presented in Figure b). Chaotic dynamics are obtained for $\Phi_0 = -0.32\,\pi$, depicted in Figure c). Other conditions are P = 3.06 and $\gamma = 0.16$.

Φ_0. We have measured the corresponding phase difference for a complete cycle of the scenario to be equivalent to π.

From the stable state, we start to decrease Φ_0 and monitor the rf-spectra of the dynamics. For decreasing Φ_0, we find the onset of periodic dynamics for $\Phi_0 \approx -0.2\,\pi$. Then, in agreement with the observations for increasing the pump parameter, a period doubling scenario evolves with a period two state for a feedback phase of $\Phi_0 = -0.24\,\pi$. This state is illustrated in Figure 4 b). Further decreasing Φ_0 effects chaotic dynamics via a period doubling route to chaos. The rf-spectrum obtained for chaotic dynamics is depicted in Figure 4 c). Approximately 10 indistinguishable cycles of this scenario can be identified for changing the voltage supplied to the PZT. We have investigated the dependence on Φ_0 for various pump parameters and found very good agreement for the dynamics with the results obtained for variations of the pump parameter. Therefore, we conclude that the observed cyclic scenario can be attributed to the feedback phase Φ_0.

This crucial dependence of the dynamics of the SL-system on Φ_0 is in agreement with results presented for SCR dynamics in references (Heil *et al.*, 2001; Heil *et al.*, 2003). However, the strong dependence on Φ_0 and the emergence of a cyclic scenario are the only similarities. Here, and in contradiction to the well-known SCR

dynamics, where the route to chaos is a quasi periodic route, we find a different route to chaos, namely, a period doubling route. Furthermore, the pronounced optical broadband dynamics, originating from a multitude of strongly interacting modes, which is realized by the resonant coupling condition, are unique for the present system. The interactions between the high number of longitudinal modes giving rise to this extraordinary optical broadband dynamics need to be identified.

4 Interactions of the Longitudinal Modes for Optical Broadband Dynamics

In order to gain insight into the interactions between the longitudinal modes, we analyze the pronounced optical broadband dynamics in detail. Therefore, we accomplish a more sophisticated experiment, in which we measure both the total intensity dynamics, comprising the dynamics of all the longitudinal modes, and the dynamics of spectrally filtered regions, consisting of only 7 longitudinal modes, simultaneously. The spectral filtering is realized by utilizing a grating monochromator, as illustrated in Figure 1. In the experiment, we compare the total intensity dynamics with the spectrally filtered dynamics at different spectral positions. We have chosen a moderate feedback rate of $\gamma = 0.18$ and a moderate pump parameter, being P = 2.52. For these conditions, we have adjusted Φ_0 for maximum optical bandwidth and broadband chaotic dynamics. The results are given in Figure 5. In this figure, the total dynamics are presented in grey, while the spectrally filtered dynamics are represented in black. In order to allow for comprehensive information, we depict the optical spectra together with the corresponding rf-spectra and 15 ns segments of the time series of the intensity dynamics. This is accomplished for three different spectral positions for the filtered dynamics. As it can be seen in the optical spectra in the Figures 5 a1), b1) and c1), the total intensity dynamics comprises a high optical bandwidth of approximately 7 nm, while the 3 dB bandwidth of the filtered dynamics can be determined to 350 pm, which corresponds to a number of 7 longitudinal modes. The series for the three different center frequency, being 781.7 nm, 784.8 nm and 787.3 nm, are depicted in rows a, b, and c, respectively.

We begin with a comparison of the total dynamics and the filtered dynamics for a filter position near the center wavelength of the optical spectrum at 784.8 nm (series b). In Figure 5 b2), the rf-spectra of the filtered dynamics reveal distinct low frequency dynamics for frequencies below 1 GHz. Such low frequency components are not present in the rf-spectrum of the total dynamics. In contrast to this, both rf-spectra show good agreement for higher frequencies between 2 GHz and 5 GHz. A comparison of the corresponding time series, which are presented in Figure 5 b3), underlines this property by revealing a clear correlation. In the time series for the filtered dynamics, we find slow intensity fluctuations on a scale of several ns. These slow fluctuations are lacking in the time series of the total dynamics. This property gives evidence for anti-phase dynamics of the many longitudinal modes on a time scale of up to several hundred MHz, a property which has been observed for various multimode SL-systems (Uchida *et al.*, 2001; Buldú *et al.*, 2002; Masoller *et al.*, 2005). In many cases thereof, mode competition has been identified for being the relevant mechanism, induced by the coupling of the modes via common gain. In contradiction to the anti-phase dynamics at low frequencies, we find in-phase dynamics in the time series for the fast sub-ns time scale pulsations. This property has also been reported for other multimode SL-systems (Uchida *et al.*, 2001). For those systems, it has been shown that the in-phase dynamics is related to the relaxation oscillation frequency of the system. However, in the present SL-system and for this pump parameter, the relaxation oscillation frequency of the solitary SL has been determined to be $\nu_{\mathrm{RO}} = 2.6\,\mathrm{GHz}$, which differs significantly from the peak at 3.5 GHz visible in the rf-spectrum.

An interesting question is if and how the dynamics of the longitudinal modes changes in other spectral regions apart from the center of the optical spectrum. Therefore, we have first decreased the center frequency of the filtered dynamics to 781.7 nm and then increased the center frequency of the filter to 787.3 nm, respectively. The corresponding results are presented in Figure 5 in series a) and in series c). We point out, that in the flanks of the optical spectrum the power of the dynamics is approximately 8 dB less, if compared to the central region of the optical spectrum, which needs to be considered for comparison of the rf-spectra of different spectral regions. Again, the corresponding rf-spectra reveal distinct low frequency dynamics, similar to the case of the center of the optical spectrum in Figure 5 in series b). Although the power of the intensity dynamics is just sufficient for detection, we find evidence for less pronounced high frequency dynamics in the flanks of the optical spectrum, while the low frequency dynamics are well pronounced. A comparison of the corresponding normalized time series, which are depicted in the Figures 5 a3) and 5 c3), underlines this result. Still, we are able to identify low frequency intensity dynamics, while the fast intensity pulsations are less pronounced than in Figure 5 b3). Furthermore, we hardly identify in-phase dynamics in time series in the Figures 5 a3) and 5 c3). These results indicate that mode competition is a relevant mechanism for all longitudinal modes involved in the dynamics, while dynamics on faster time scales exceeding 1 GHz originates rather from near the center region of the optical spectrum.

However, a relevant question has been brought up by these results concerning the nature of the pronounced multimode dynamics. Namely, whether the dynamics is inherently broadband for all longitudinal modes disregarding the spectral position, or whether the dynamics in the center drives the dynamics in spectrally

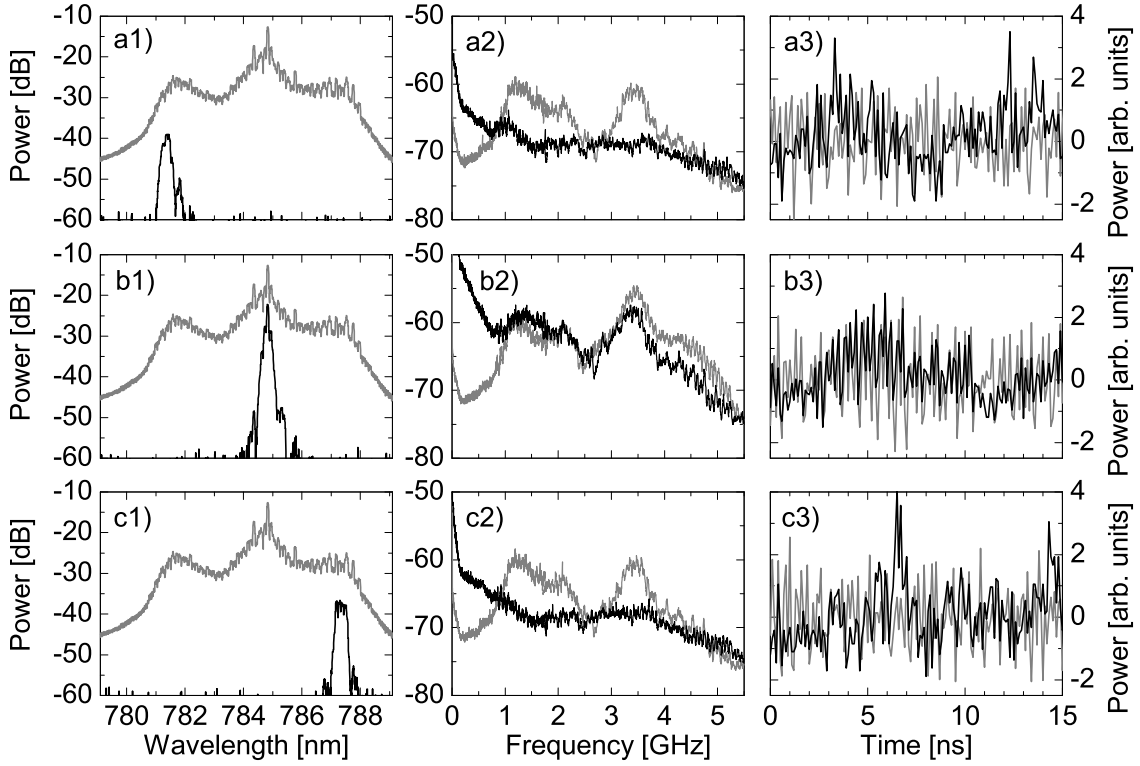

Figure 5. Comparison of total and spectrally filtered dynamics for optical broadband emission dynamics. The dynamics for three different center frequencies of the filter, which are 781.7 nm in a), 784.8 nm in b) and 787.3 nm in c), are shown. Total dynamics are represented in gray and filtered dynamics in black. The optical spectra are depicted in a1), b1) and c1), while the corresponding rf-spectra and normalized time series are presented in a2) - c2) and a3) - c3), respectively. The pump parameter is P = 2.52 and the feedback rate amounts to $\gamma = 0.18$.

distant regions. This inevitably leads to the question, whether information is (equally) produced in a collective manner in the whole spectral range, or if information is produced in the center and successively flows to spectrally distant regions? Further experiments are required in order to answer this question and other open questions providing important information about the relevant mechanisms for such dynamics. Additionally, analysis of suitable models is a desirable and complementary approach to achieve this goal, which has been proven as powerful for conventional SL-systems. However, a suitable model accounting for the relevant property of resonant coupling is currently not available.

5 Conclusion

We have studied a SL-system with comparable length of the external cavity and the laser cavity. For resonant coupling conditions, we have identified that the dynamics strongly depend on the feedback phase. For continuously changing feedback phase, we have revealed a cyclic scenario with dynamics evolving from stable emission to periodic states, then to chaotic dynamics, and back to stable emission. At first sight, these findings are similar to the properties reported for conventional short cavity regime (SCR) SL-systems, which can be modeled by Lang-Kobayashi (LK) equations. Nevertheless, we have demonstrated distinct differences in the route to chaos and in the characteristics of the chaotic dynamics if compared to conventional SCR-dynamics. A remarkable property of the system presented is that the system allows for the generation of broadband chaotic intensity dynamics with broadband spectral dynamics comprising an optical bandwidth of around 7 nm. For this state, we have demonstrated pronounced multimode dynamics with a number of more than 130 interacting longitudinal modes. We have compared the properties of the SL-system with respect to compatibility to models based on the LK-equations, and find that refined models are needed to understand the systems dynamics. This is mainly due to the resonant coupling condition allowing for pronounced multimode dynamics. Finally, we associate the onset of the observed optical broadband dynamics to spectral overlap between longitudinal modes caused by feedback induced spectral dynamics.

From the nonlinear dynamics point of view, an understanding of these characteristic properties of the dynamics is desired, since identification of the underlying mechanisms might reveal general properties of complex multimode system. In this context, further experiments with this well-controllable SL-system can support relevant studies on the dynamics of pronounced multimode system. Finally, we point out that additionally to the interest in the pronounced multimode dynamics of this SL-system from a nonlinear dynam-

ics point of view, the corresponding high optical bandwidth qualifies the SL-systems for implementation in novel technical and medical applications where optical broadband light sources are required, e.g. for chaotic light detection and ranging (CLIDAR) (Lin and Liu, 2004) and coherence tomography (Brezinski and Fujimoto, 1999).

Acknowledgements

The authors thank Sacher Laser Technik GmbH, Germany, for assistance in developing the well-controllable short external cavity semiconductor laser system and gratefully acknowledge funding of this project by the German Federal Ministry of Education and Research FKZ 13N8174.

References

Brezinski, M. E. and Fujimoto, J. G. (1999). Optical coherence tomography: High-resolution imaging in nontransparent tissue. *IEEE J. Select. Topics Quantum Electron.* **STQE-5**(4), pp. 1185–1192.

Buldú, J. M., Rogister, F., Trull, J., Serrat, C., Torrent, M. C., Garcia-Ojalvo, J. and Mirasso, C. R. (2002). Asymmetric and delayed activation of side modes in multimode semiconductor lasers with optical feedback. *J. Opt. B: Quantum Semiclass. Opt.* **4**(6), pp. 415–420.

Donati, S. and Mirasso, C. R., Eds. (2002). feature section on optical chaos and applications to cryptography. *IEEE J. Quantum Electron.* **QE-38** (9).

Duarte, A. A. and Solari, H. G. (1997). Modeling the spatio-temporal dynamics of semiconductor lasers: the monochromatic solutions. *Opt. Commun.* **144**(1-3), pp. 99–108.

Fischer, I., vanTartwijk, G. H. M., Levine, A. M., Elsäßer, W., Göbel, E. and Lenstra, D. (1996). Fast pulsing and chaotic itinerancy with a drift in the coherence collapse of semiconductor lasers. *Phys. Rev. Lett.* **76**(2), pp. 220–223.

Heil, T., Fischer, I. and Elsäßer, W. (1999). Influence of amplitude-phase coupling on the dynamics of semiconductor lasers subject to optical feedback. *Phys. Rev.* **A 60**(1), pp. 634–641.

Heil, T., Fischer, I., Elsäßer, W. and Gavrielides, A. (2001). Dynamics of semiconductor lasers subject to delayed optical feedback: The short cavity regime. *Phys. Rev. Lett.* **87**(24), 243901.

Heil, T., Fischer, I., Elsäßer, W., Krauskopf, B., Green, K., and Gavrielides, A. (2003). Delay dynamics of semiconductor lasers with short external cavities: Bifurcation scenarios and mechanisms. *Phys. Rev.* **E 67**(6), 066214.

Henry, C. H. (1982). Theory of the linewidth of semiconductor lasers. *IEEE J. Quantum Electron. QE-18*2, pp. 259–264.

Koryukin, I. V. and Mandel, P. (2004). Dynamics of semiconductor lasers with optical feedback: Comparison of multimode models in the low-frequency fluctuation regime. *Phys. Rev.* **A 70**(5), 053819.

Krauskopf, B., Lenstra, D., Ed. (2000). *Fundamental Issues of Nonlinear Laser Dynamics*. Conference Proceedings Vol. 548. American Institute of Physics, Melville (N.Y.).

Lang, R. and Kobayashi, K. (1980). External optical feedback effects on semiconductor injection-laser properties. *IEEE J. Quantum Electron.* **QE-16**(3), pp. 347–355.

Larger, L. and Goedgebuer, J.-P., Eds. (2004). special issue on cryptography using optical chaos. Vol. 5/6.

Lenstra, D. (1997). Fundamental nonlinear dynamics of semiconductor lasers. *Quantum Semiclass. Opt.* **9**(5), pp. U3–U5.

Lin, F. Y. and Liu, H. M. (2004). Chaotic lidar. *IEEE J. Select. Topics Quantum Electron* **STQE-10**(5), pp. 991–997.

Masoller, C., Torre, M. S. and Mandel, P. (2005). Antiphase dynamics in multimode semiconductor lasers with optical feedback. *Phys. Rev.* **A 71**(1), 013818.

Möhrle, M., Sartorius, B., Bornholdt, C., Bauer, S., Brox, O., Sigmund, A., Steingrüber, R., Radziunas, M. and Wünsche, H.-J. (2001). Detuned grating multisection-RW-DFB lasers for high-speed optical signal processing. *IEEE J. Sel. Top. Quantum Electron.* **STQE-7**(2), pp. 217–223.

Mørk, J., Tromborg, B. and Mark, J. (1992). Chaos in semiconductor-lasers with optical feedback - theory and experiment. *IEEE J. Quantum Electron.* **QE-28**(1), pp. 93–108.

Mørk, J, Tromborg, B. and Christiansen, P. L. (1988). Bistability and low-frequency fluctuations in semiconductor-lasers with optical feedback - a theoretical-analysis. *IEEE J. Quantum Electron.* **QE-24**(2), pp. 123–133.

Sukow, D. W., Heil, T., Fischer, I., Gavrielides, A., Hohl-AbiChedid, A. and Elsäßer, W. (1999). Picosecond intensity statistics of semiconductor lasers operating in the low-frequency fluctuation regime. *Phys. Rev.* **A 60**(1), pp. 667–673.

Tromborg, B., Mørk, J. and Velichansky, V. (1997). On mode coupling and low-frequency fluctuations in external-cavity laser diodes. *Quantum Semiclass. Opt.* **9**, pp. 831–851.

Uchida, A., Liu, Y., Fischer, I., Davis, P. and Aida, T. (2001). Chaotic antiphase dynamics and synchronization in multimode semiconductor lasers. *Phys. Rev.* **A 64**(2), 023801.

vanTartvijk, G. H. M., Levine, A. M. and Lenstra, D. (1995). Sisyphus effect in semiconductor-lasers with optical feedback. *IEEE J. Select. Topics Quantum Electron.* **STQE-1**(2), pp. 466–472.

Yousefi, M., Barsella, A., Lenstra, D., Morthier, G., Baets, R., McMurtry, S. and Vilcot, J. P. (2003). Rate equations model for semiconductor lasers with multilongitudinal mode competition and gain dynamics. *IEEE J. Quantum Electron.* **QE-39**(10), pp. 1229–1237.